Propylamine Silica-Titania Hybrid Material Modified with Ni(II) as the Catalyst for Benzyl Alcohol to Benzaldehyde Conversion

Dewi Agustiningsih, Nuryono Nuryono, Sri Juari Santosa, and Eko Sri Kunarti*

Department of Chemistry, Faculty of Mathematics and Natural Sciences, Universitas Gadjah Mada, Sekip Utara, Yogyakarta 55281, Indonesia

Corresponding author:

tel: +62-81578634638
email: eko_kunarti@ugm.ac.id

Received: May 8, 2023
Accepted: June 15, 2023

DOI: 10.22146/ijc.84282

Abstract: *SiO_2-TiO_2@propylamine-Ni(II) as the catalyst for the benzyl alcohol oxidation has been synthesized by utilizing rice husk ash as the SiO_2 source. This research was started by extracting SiO_2 from rice husk ash and continued by synthesizing the SiO_2-TiO_2 composite using titanium(IV) tetraisopropoxide (TTIP) as TiO_2 precursor and PEG-40 as template. The composite functionalization and metal modification were carried out by adding (3-aminopropyl)triethoxysilane (APTES) as the source of propylamine linker and impregnating $NiCl_2{\cdot}6H_2O$ as the nickel precursor, respectively. The catalysts were synthesized by varying the ratios between each component within the material. The prepared materials were then characterized using ATR-IR, XRD, XRF, PSA, SAA, AAS, SEM-EDX, HR-TEM, and TGA. The catalyst activity was investigated by applying it to the oxidation reaction of benzyl alcohol to benzaldehyde with H_2O_2 as the oxidizing agent under sonication system. The obtained products were then analyzed by using GC-MS to quantify the success of the reaction. All characterizations performed in this research generally indicate the success in the synthesis of SiO_2-TiO_2@propylamine-Ni(II) materials. Under the same condition including at room temperature, 1 h reaction time, and sonication system, the optimal oxidation reaction of benzyl alcohol was reached when SiO_2-TiO_2@propylamine-Ni(II)5 was used as the catalyst in 98.52% yield.*

Keywords: *benzaldehyde; benzyl alcohol; catalyst; oxidation reaction; SiO_2-TiO_2@propylamine-Ni(II)*

■ INTRODUCTION

Alcohol oxidation to many forms of carbonyl-based compounds is one of the vast significances to the development of chemical fabrication [1]. The most notable example is the conversion of benzyl alcohol to benzaldehyde, which provides numerous applications in diverse areas such as coloring agents, medical products, farming, fragrances, foods, drinks, and also chemicals [2]. Most of the aldehyde is produced by a selective oxidation mechanism of alcohol utilizing a homogeneous catalyst. However, this kind of method has some drawbacks, including low reusability, difficult separation, low degree of conversion, and toxic contaminants [3-4]. As a result, it is essential to find an environmentally friendly and effective method to replace the homogeneously catalyzed oxidation reaction. Noble metals such as gold, platinum, and palladium have long been developed as heterogeneous catalysts in benzyl alcohol to benzaldehyde oxidation reactions. These metals are generally dispersed onto supporting materials and have been observed to have significant catalytic activity [5-6]. Regrettably, the noble metal precludes its widespread potential for application due to its rising cost. Non-noble metals with a lower cost, such as nickel, can be used and have been reported to be advantageous for benzyl alcohol oxidation [7-9].

A catalyst based on nickel metal dispersed on SiO_2-TiO_2 composite was used in this study. Silica was chosen because it has several advantages, including the ability to form a large framework, abundance in nature and living creatures, great efficiency, selectivity, surface area, thermal stability, also good mechanical properties. Even

so, silica has a limitation as a support material since it forms inadequate compatibility with transition metals, limiting its interaction with these metals. Consequently, the transition metals are distributed poorly on the surface [10]. This major silica limitation can be overcome by combining silica with other metal oxides, one of which is titania. This is driven by the fact that titania can interact well with almost all transition metals, including Au, Cu, Ni, Mn, Pd, Co, and Ru. Titania also has high thermal and chemical stabilities [11]. The optimal interaction between titania and metal will aid the interaction of silica and metal. Hence, combining silica and titania into a composite should result in a support material with high thermal stability, a large surface area, and the ability to interact optimally with the catalyst metal.

Rice husk ash will be used as a silica source in this research. This is owed to the fact that rice husk ash contains silica with a very high purity level of 94–99% [12-13]. There are already so many reported studies about SiO_2 extraction from rice husk ash, including its application as a cement component [14-18], geopolymer [19-23], functional material [24], microelectronic, sensor, nano additives [25], adsorption and filtration membrane [26], photocatalyst [27], bioimaging, as well as drug delivery agent [28]. Despite its extensive utilization and application, there has not been found previous research which addressed the simultaneous modification of silica extracted from rice husk ash with TiO_2 and APTES linker agent as had been conducted in this research.

Even though the SiO_2-TiO_2 composite has the potential to become an excellent supporting material, there is still a drawback, such as the metal can be easily leached from the composite surface due to the weak physical interaction. This, of course, brings down the activity of the catalyst in the benzyl alcohol oxidation reaction. This problem can be fixed by incorporating organic linker agents such as imines, amines, and oleic acid onto the composite surface to become inorganic-organic hybrid material [29]. The optimal interaction of the metal and the functionalized linker agent on the surface of the supporting material will augment the catalyst stability. In this study, the compound (3-aminopropyl)triethoxysilane was utilized as the source of propylamine linker agent between the metal ion catalyst and the SiO_2-TiO_2 composite. Moreover, the sonication method was conducted in the oxidation reaction of benzyl alcohol to benzaldehyde as the application of this research. This method was used owing to its ability to accelerate the reaction and lower the required reaction temperature [30].

■ EXPERIMENTAL SECTION

Materials

The materials used in this research were pro-analysis quality chemicals purchased from Sigma-Aldrich and Merck including HCl 37%, NaOH, Na_2SO_4 99.9%, $C_9H_{23}NO_3Si$ 99%, $Ti\{OCH(CH_3)_2\}_4$ 97%, PEG-40, C_2H_5OH 99%, $NiCl_2{\cdot}6H_2O$ 99.9%, $C_6H_5CH_2OH$ 99%, and H_2O_2 30%. Other technical-grade materials were used, including distilled water and rice husk ash obtained from Semarang, Central Java. No further purification was conducted for all used reagents.

Instrumentation

The instrumentations used for the characterization in this study include attenuated total reflectance-infrared spectroscopy (QATR 10, Shimadzu), X-ray diffractometer (XRD-6000, Shimadzu), scanning electron microscope-energy dispersive X-ray (JEC-3000 FC, JEOL), high resolution-transmission electron microscope (Tecnai G^2 20 S-Twin, FEI), thermogravimetric analyzer (STAR^e SW, METTLER), X-ray fluorescence (NEXQC$^+$, QUANTEZ), particle size analyzer (SZ-100, HORIBA Scientific), surface area analyzer (Gemini VII Version 5.03, Micromeritics), atomic absorption spectroscopy (iCE 3000 AA01212502, Thermo Scientific), and gas chromatography-mass spectrometer (QP2010S, Shimadzu).

Procedure

Extraction of SiO_2 from rice husk ash

Rice husk ash (RHA) was leached by dissolving it in 1 M HCl at a ratio of 1:10 (w/v). The mixture was stirred at room temperature for 2 h before being washed with distilled water. The RHA was then dried for 8 h at 80 °C before being calcined for 5 h at 550 C. Next, ATR-

IR, XRD, and XRF methods were used to characterize the uncalcined and calcined RHA. To extract the silica, the calcined RHA was then dispersed in 1 M NaOH with a ratio of 1:10 (w/v) and stirred for 2 h at 90 °C. It was next followed by centrifugation at 4000 rpm for 20 min. Afterward, the sodium silicate liquid was then collected as the silica precursor to be used in the next procedure.

Synthesis of SiO_2-TiO_2 composite

To synthesize the SiO_2-TiO_2 composite, 1 mol of sodium silicate was neutralized with 1 M HCl dropwise until a neutral pH was reached. Next, 1 mol of TTIP precursor was dispersed in absolute ethanol at 1:1 (v/v) ratio. The dispersed TTIP in ethanol was then added to the silica gel that had been formed before in the sonication system. The composite was then added dropwise with PEG-40 at a mol ratio of 1:6 (PEG:composite). The mixture of silica, titania, and PEG-40 was sonicated for 1 h to produce a white suspension prior to getting dried at 80 °C for 24 h. The template removal process was completed by dispersing SiO_2-TiO_2@PEG in absolute ethanol with a ratio of 1:10 (w/v) in a sonication system for 1 h at room temperature. The solid was then filtered, washed with cold absolute ethanol, and dried for 8 h at 60 °C. The same procedure was carried out to remove the template twice.

Functionalization of SiO_2-TiO_2 composite

The functionalization procedure was conducted by dispersing SiO_2-TiO_2 composite in absolute ethanol at 1:10 (w/v) ratio. The propylamine with the mass ratio of 1:2 (w/w) to SiO_2-TiO_2 was also then dispersed in ethanol 1:10 (v/v). The propylamine solution was gradually added to the composite mixture before being sonicated for 2 h and stirred for 6 h at room temperature. Just after that, centrifugation was performed to obtain the solid. It was then filtered before being washed with absolute ethanol and distilled water three times for each, afterwards dried at 60 °C for 12 h [31].

Metal impregnation of SiO_2-TiO_2@propylamine hybrid material

As much as 1 g of SiO_2-TiO_2@propylamine hybrid material was dispersed in distilled water with a ratio of 1:100 (w/v) and then added with nickel(II)-chloride hexahydrate in various moles. The mixture was sonicated for 3 h at room temperature before being filtered and washed three times with distilled water. The obtained greenish-white solid was then dried for 4h at 80 °C, and finally characterized using ATR-IR, XRD, PSA, SAA, AAS, SEM-EDX, HR-TEM, and TGA.

Catalytic activity

In the oxidation reaction of benzyl alcohol, as much as 1 mmol of benzyl alcohol, 50 mg of catalyst material, and 1 mL of H_2O_2 were added into a vial. The reaction was carried out for 1 h at room temperature in a sonication system [2]. When the reaction finished, the solid catalyst was restored through the filtration process. Next, the organic phase was extracted from the filtrate and dried using anhydrous sodium sulfate. Lastly, the final products were then analyzed with GC-MS.

■ RESULTS AND DISCUSSION

Characterization of SiO_2 from RHA

From Table 1, it is reported that rice husk ash has a high content of silica up to 97.923%. It supports the known fact that rice husk ash is one of the most potential silica natural sources. According to the results of the ATR-IR characterization in Fig. 1, there are peaks in the spectra of the uncalcined RHA that indicate the dominant carbon component. These peaks include 1373 (Csp^3–H bending), 1600 (C=C aromatics), 1743 (C=O stretching), 2939 (Csp^3–H stretching), and 3424 cm^{-1} (O–H stretching). Some peaks also indicate the presence of silica in uncalcined RHA, such as 432 (SiO_4 bending mode), 794 (Si–O–Si symmetrical stretching), and 1049 cm^{-1} (Si–O–Si asymmetrical stretching). After the rice husk ash had been leached and calcined, the carbon

Table 1. Composition of calcined rice husk ash

Component	Content (%mass)
SiO_2	97.923
Fe_2O_3	0.388
K_2O	0.784
CaO	0.647
TiO_2	0.121
MnO	0.079
Cr_2O_3	0.031

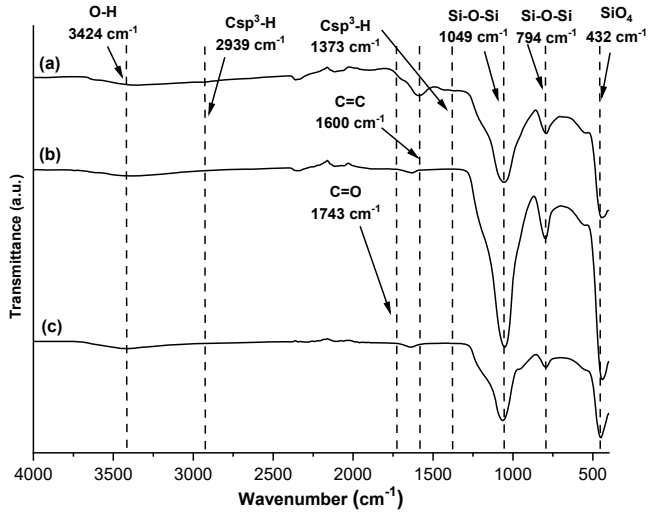

Fig 1. ATR-IR spectra of (a) uncalcined RHA, (b) calcined RHA, and (c) extracted silica

component began to disappear. It is evidenced by the decreasing intensity of the carbon material characteristic peaks and the increasing relative intensity of silica characteristic peaks. Based on these results, it can be concluded that the calcination process to remove the carbon component in rice husk ash was successfully done. The ATR-IR spectra of silica extracted from rice husk ash reveal that it contained high purity. This is clearly indicated by some characteristic peaks belonging to pure silica.

Fig. 2 depicts that calcined and uncalcined RHA exhibit a characteristic pattern of amorphous silica with a broad peak at 2θ around 22°. Moreover, it can be noticed here that the intensity of these peaks increases in leached and calcined rice husk ash spectra. It can be explicated by the fact that metal oxides other than SiO_2 were dissolved after leaching, and the amount of carbon in rice husk ash decreased after calcination. The loss of other metal oxides and carbon increased the relative intensity of the broad peaks from amorphous SiO_2. The pattern from the extracted silica displays higher intensity and more distinct peaks compared to other spectra in the same region, providing confirmation that it was purely derived from calcined RHA.

Characterization of SiO_2-TiO_2 before and after Template Removal

The method used in the synthesis of the SiO_2-TiO_2 composite was sol-gel by adding TTIP precursor to the obtained silica gel. The mixture was then treated with polyethylene glycol 40 (PEG-40) as the template. PEG is the most used surfactant as a template due to its non-toxic long polymeric chain and good water solubility [32]. It is also known to have good properties such as hydrophilic, water-soluble, biocompatible, non-toxic, and protein-resistant [33]. Subsequently, to produce the SiO_2-TiO_2 composite, this template must be removed. Instead of calcination, the template removal process in this study was carried out using the sonication method. It was done to prevent exposing the composite to high temperatures, which might result in the formation of crystalline phases for both SiO_2 and TiO_2. If a crystalline phase is formed, the number of free silanol and titanol groups on the surface tends to decrease because they are used to form crystalline structures. This is disadvantageous since these groups are required for bond formation with propylamine as the interparticle linker agent in the next step.

Fig. 3 shows the ATR-IR spectra of the SiO_2-TiO_2 composite before and after the template removal. Some characteristic peaks of the composite are detected including at 3400 (O–H stretching of the silanol and titanol groups), 2924 (Csp^3–H stretching), 1735 (C=O stretching), 1643 (O–H bending from SiO–H), 1465 (Csp^3–H bending for $–CH_2–$), 1350 (Csp^3–H bending for $–CH_3$), 1049 (Si–O–Si asymmetrical stretching), 794 (Si–O–Si symmetrical stretching), and 949 cm^{-1} (Si–O–Ti stretching). After the sonication for template removal

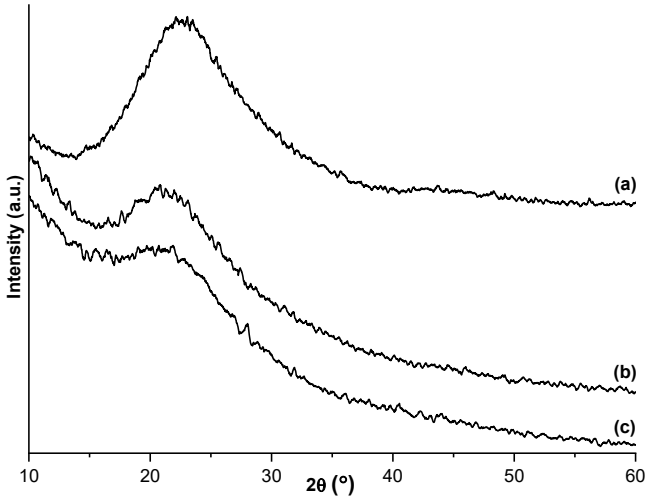

Fig 2. X-ray diffraction pattern of (a) extracted silica, (b) calcined RHA, and (c) uncalcined RHA

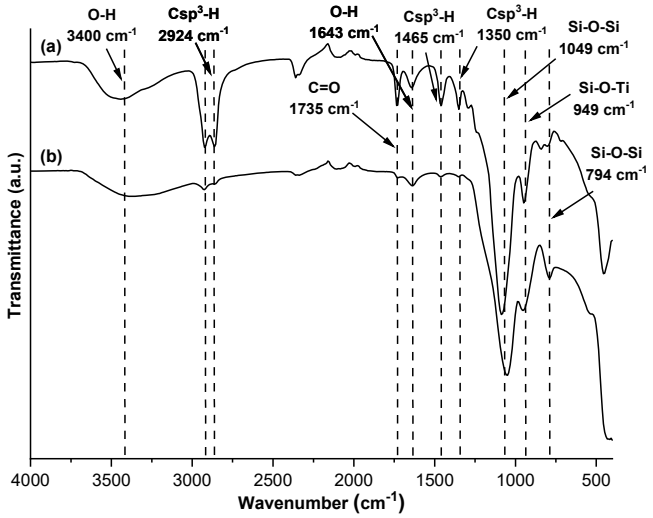

Fig 3. ATR-IR spectra of (a) SiO_2-TiO_2@PEG-40 and (b) SiO_2-TiO_2 after PEG-40 removal

was carried out, the intensity of PEG-40 characteristic peaks comprising 2924 (Csp^3–H stretching), 1735 (C=O stretching), 1465 (Csp^3–H bending for $–CH_2–$), and 1350 cm^{-1} (Csp^3–H bending for $–CH_3$) significantly decrease. Based on the difference in mass before and after template removal, the sonication method could remove up to 88.92% of the template at SiO_2-TiO_2 composite.

According to Fig. 4, the ATR-IR characterization results for the propylamine functionalized composite do not show significant differences from the composite spectra prior to functionalization. However, if we take a closer look, we can see differences in the shape and intensity of the peak at 1550 cm^{-1}. There is no vibration peak around that wavenumber prior to functionalization. Then after functionalization, a broad peak is observed, indicating the presence of the $–NH_2$ group deformation vibration in propylamine from APTES [34-35]. After functionalization, the Ti–O–Si vibrational peak appeared to merge with the Si–O–Si peak. The probable answer for this case is that when APTES was added to the composite, the silane groups preferred to bind with silanol groups to form Si–O–Si rather than with titanol groups to form Si–O–Ti. This is most likely since the same size of Si from silane and silanol would optimize the orbital overlap that occurred during the bond formation. Meanwhile, the size difference between Si and Ti shrunk the probability of orbitals overlapping.

The ATR-IR spectra of propylamine-functionalized and Ni(II)-impregnated SiO_2–TiO_2 in Fig. 5 reveal the characteristic peak of the Ni–N bond at 410–420 cm^{-1} [36]. This peak suggests that nickel ion was successfully dispersed on the composite surface through the formation of the bond between nickel ion from precursor salt and nitrogen atom belonging to the amine groups from propylamine resulted by APTES.

Based on Fig. 6(b), the diffraction pattern of the composite after template removal exhibits the amorphous properties of silica and titania at 2θ 22°. This suggests that both silica and titania were obtained as amorphous materials rather than crystalline. It is presumably because the growth of silica and titania crystals did not

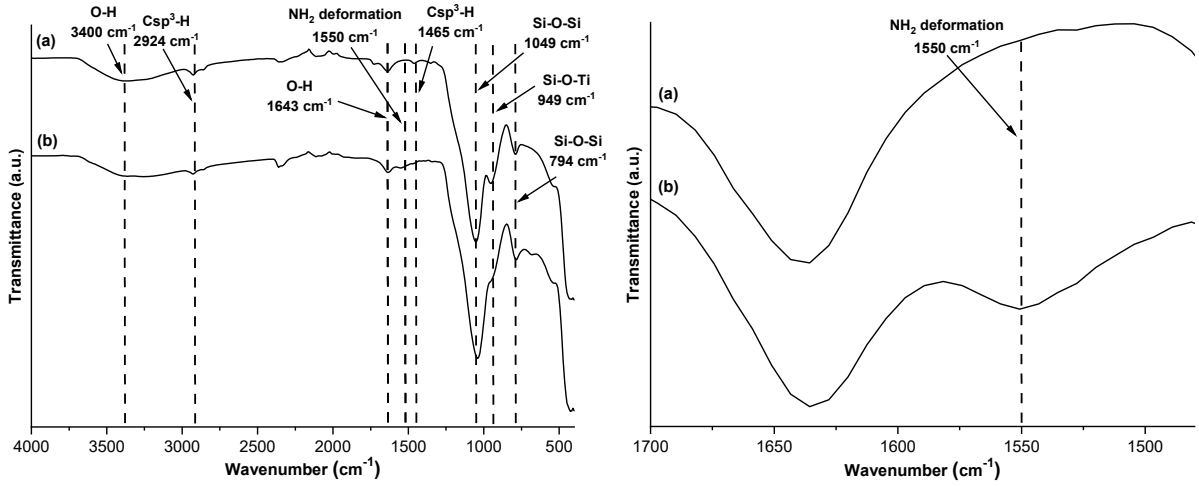

Fig 4. ATR-IR spectra of (a) SiO_2-TiO_2 and (b) SiO_2-TiO_2@propylamine

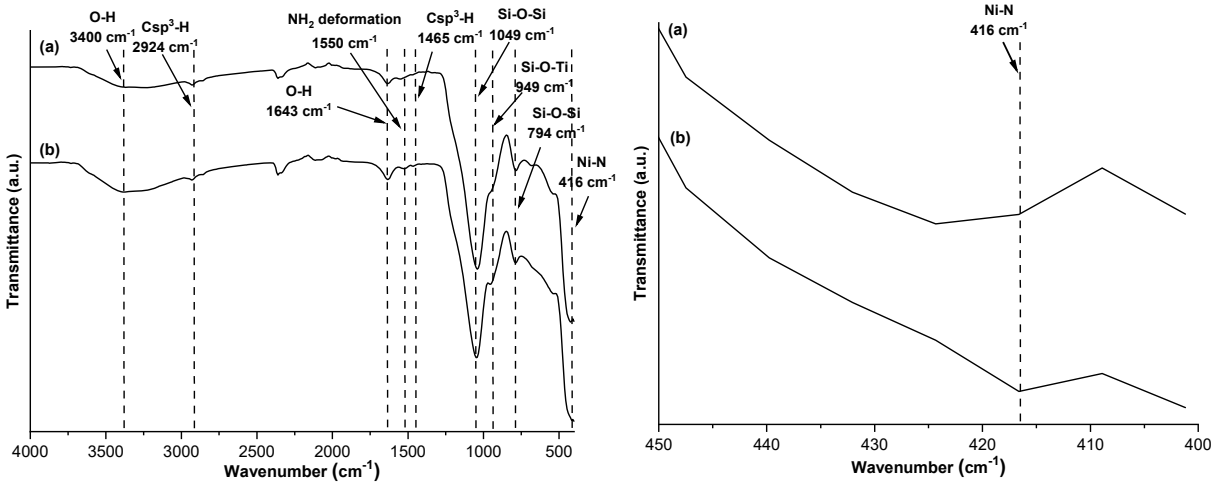

Fig 5. ATR-IR spectra of (a) SiO_2-TiO_2@propylamine and (b) SiO_2-TiO_2@propylamine-Ni(II)

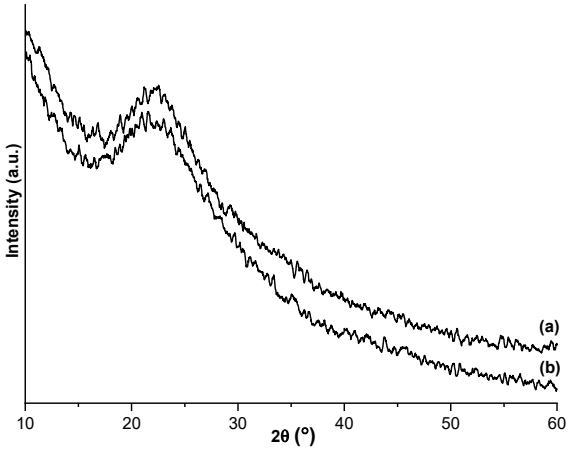

Fig 6. X-ray diffraction pattern of (a) SiO_2-TiO_2@propylamine-Ni(II) and (b) SiO_2-TiO_2

occur when calcination at high temperatures was not executed during the template removal process. In addition, Fig. 6(a) depicts that the diffraction pattern of SiO_2-TiO_2@propylamine-Ni(II) seems to have an identical amorphous character, and no other additional peaks are observed. It can be explained by two probable reasons, including (i) propylamine from APTES did not contribute to the provision of diffraction patterns, and (ii) the formed nickel in this material was Ni(II). The Ni(II) metal ions did not exhibit a specific diffraction pattern since there was no crystal growth in it [37].

As it is shown in Fig. 7, the average size of SiO_2-TiO_2 particles beyond the nano dimension (more than 100 nm) is 1365 nm. The formation of sufficiently large particles was driven by the fact that both titania and silica were in the amorphous phase. The amorphous phase is known to have a greater particle coalescence or agglomeration rate than the crystalline one [38]. Moreover, it can also be noticed here that the presence of APTES and Ni(II) metal ions could decrease the probability of aggregation among the composite particles with an average size of 662 nm. This effect was likely attributed to the capping action exerted by these two modifiers on the surface of the composite.

Based on SAA data, the SiO_2-TiO_2 composite exhibited a surface area of 234.0573 m^2/g and an average pore size of 7.28 nm. Subsequently, upon the addition of APTES and Ni(II), the composite experienced an augmentation in surface area, 243.9891 m^2/g, alongside a reduction in average pore size, 6.81 nm. The increase in

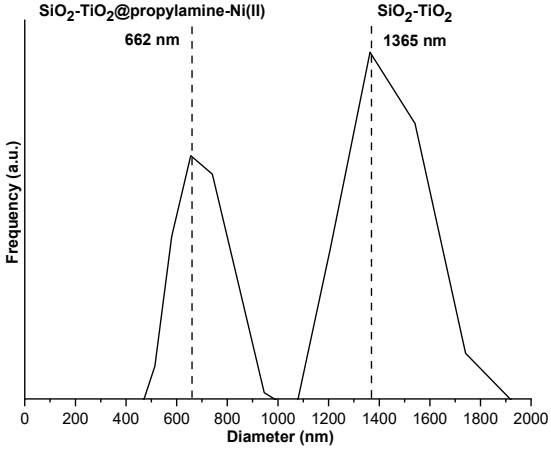

Fig 7. Particle size distribution spectra of the synthesized materials

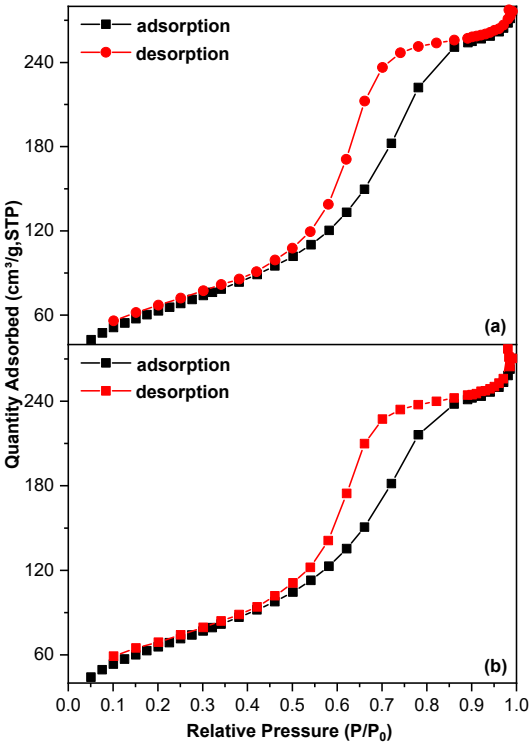

Fig 8. N_2 adsorption-desorption isotherm of (a) SiO_2-TiO_2 and (b) SiO_2-TiO_2@propylamine-Ni(II)

surface area could be caused by the presence of metal ions that enhanced the composite roughness and abruptness. Meanwhile, the pore size continued to decrease due to the closure of pores resulting from the presence of APTES and Ni(II) on the surface. In addition, as shown in Fig. 8(a) and (b), the N_2 adsorption-desorption isotherm curves of these two materials illustrate type IV hysteresis as the characteristic type of mesoporous material. The formed pore sizes are generally greater than 5 nm, indicating that the materials may be used as catalyst in the organic reaction of converting benzyl alcohol to benzaldehyde.

Fig. 9(a) and (b) display the TGA analysis results, indicating two distinct instances of mass loss for the material. The initial mass reduction was attributed to the evaporation of water molecules from the material surface, while the second event arose from the elimination of organic components derived from propylamine. Additionally, it is evident that the composite containing Ni(II) exhibited a lower mass loss compared to the composite without it. In simpler terms, this suggests that the presence of Ni(II) metal ions enhanced the thermal stability of the material. This could be owing to the thermal conductivity properties of nickel as metal, enabling it to restrict the entry of heat into the catalyst material system.

Characterization of SiO_2-TiO_2@propylamine-Ni(II) with Various Amounts of Ni(II)

As can be seen in Fig. 10, each catalyst material with various nickel ion concentrations exhibits a sharp peak in the 1500–1550 cm^{-1} region with the addition of propylamine. Further to that, the peaks between 410 and 420 cm^{-1} are also observed, indicating the Ni–N bond. The Ni–N peak intensity belonging to the catalyst material containing 5 mmol of nickel ion is greater than the others. When the nickel ion concentration in the material reached the upper 5 mmol, the peak intensity decreased. It is because even though the amount of N

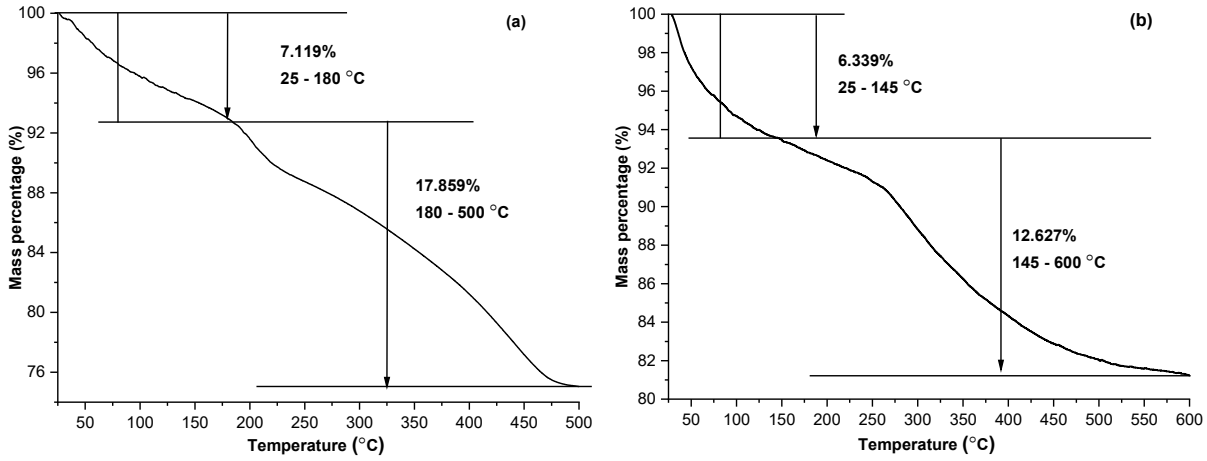

Fig 9. TGA curve of (a) SiO_2-TiO_2@propylamine and (b) SiO_2-TiO_2@propylamine-Ni(II)

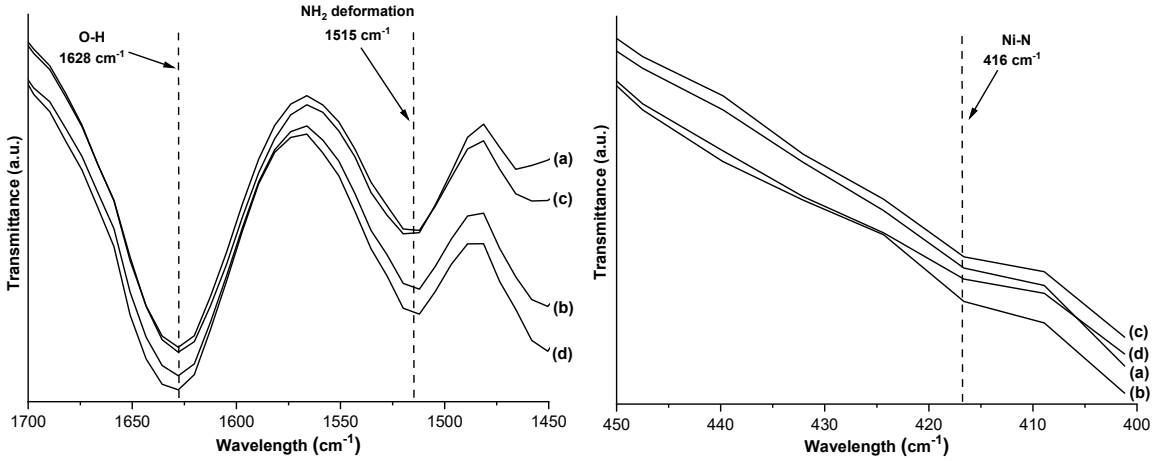

Fig 10. ATR-IR spectra of SiO_2-TiO_2@propylamine-Ni(II) with nickel ion concentrations of (a) 3; (b) 5; (c) 7; and (d) 10 mmol

available from propylamine remained constant, there was more competition between Ni atoms to bind to N. The quantitative analysis results by AAS displayed in Fig. 11 are analogous to the results from this ATR-IR characterization. It is that the optimal amount of successfully attached nickel ion was found in the SiO_2-TiO_2@propylamine-Ni(II) (5 mmol) catalyst.

According to the XRD data depicted in Fig. 12, all materials have amorphous SiO_2-TiO_2 diffraction patterns. The difference in nickel ion concentrations had no effect on the changes in SiO_2-TiO_2 diffraction pattern, as the metal ions were only dispersed on the outside of the framework. Thus, it had no role in the main framework of the SiO_2-TiO_2 amorphous structure.

As we can see from the SEM data shown in Fig. 13, the morphology of the obtained composites is generally spherical with the grain size of more than 100 nm. In addition, from Table 2, it is known that constituent elements such as Si, Ti, C, O, Ni, and N are detected in each composite based on the EDX data. Fig. 14(a) displays the HR-TEM image of SiO_2-TiO_2@propylamine-Ni(II) particles with 5 mmol nickel ions. It has a quasi-spherical shape with propylamine covering each particle, and the area defined is represented

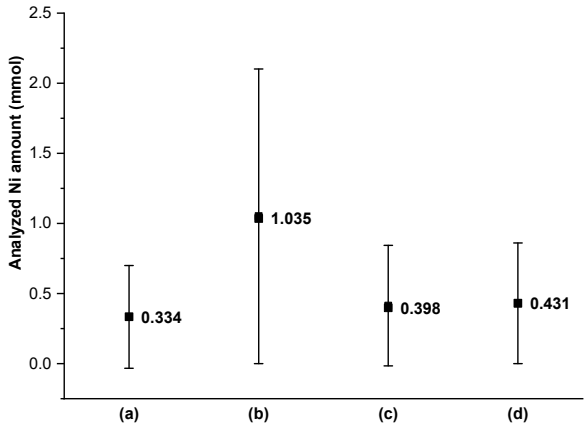

Fig 11. The amount of attached Ni in SiO_2-TiO_2@propylamine-Ni(II) with initial nickel ion concentrations of (a) 3; (b) 5; (c) 7; and (d) 10 mmol by AAS analysis

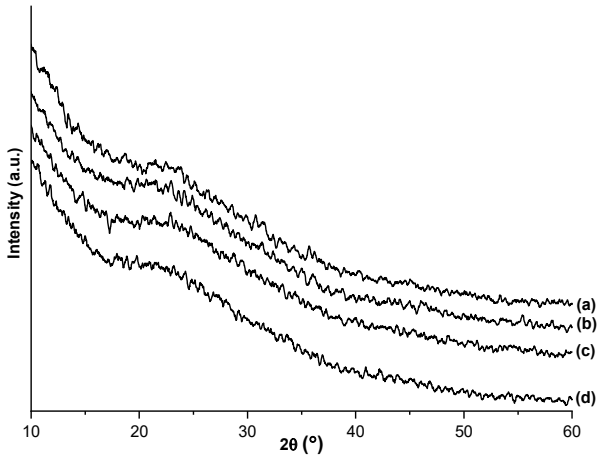

Fig 12. X-ray diffraction pattern of SiO_2-TiO_2@propylamine-Ni(II) with nickel ion concentrations of (a) 3; (b) 5; (c) 7; and (d) 10 mmol

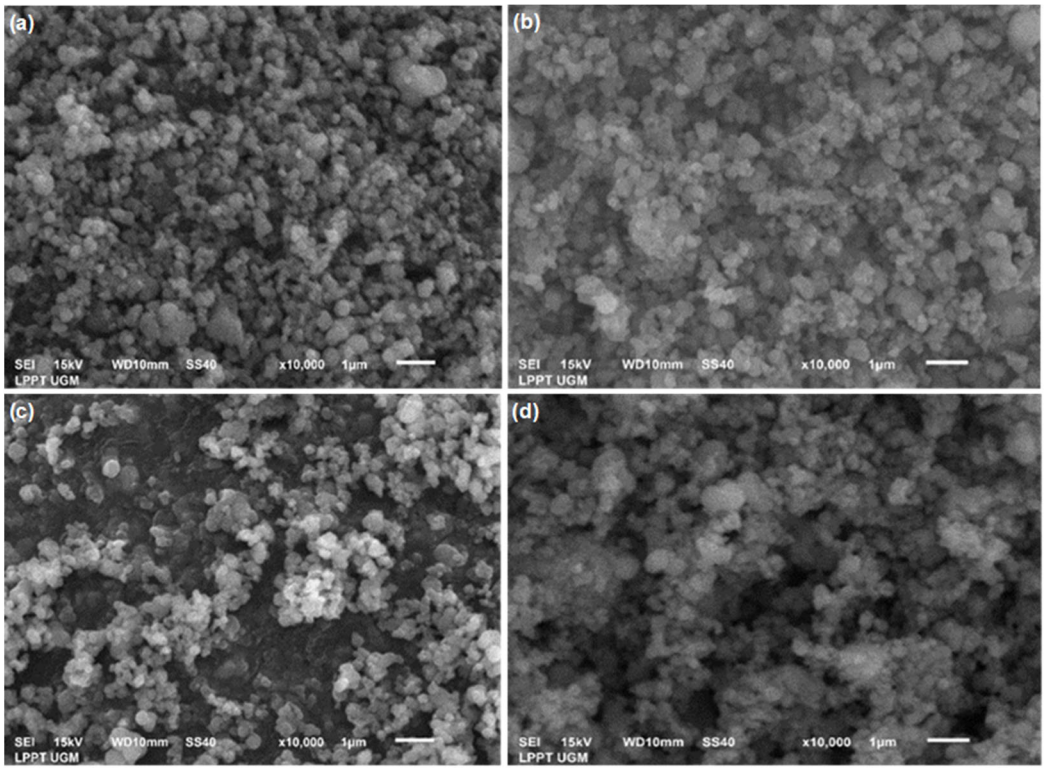

Fig 13. SEM images and EDX spectra of SiO_2-TiO_2@propylamine-Ni(II) with nickel ion concentrations of (a) 3; (b) 5; (c) 7; and (d) 10 mmol

Table 2. Percentage of the detected elements in catalyst materials by EDX

SiO_2-TiO_2@propylamine-Ni(II)	Si	Ti	C	O	Ni	N
Ni(II) 3 mmol	30.31	11.90	4.50	40.19	1.27	11.83
Ni(II) 5 mmol	11.36	27.16	9.58	45.13	2.91	3.86
Ni(II) 7 mmol	16.79	24.28	8.01	47.09	2.42	1.41
Ni(II) 10 mmol	18.45	20.49	7.74	45.30	3.67	4.35

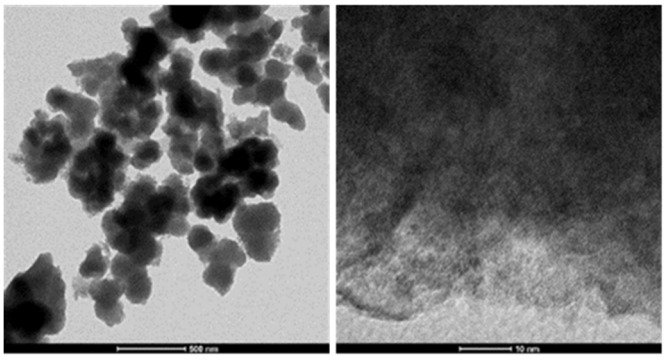

Fig 14. HR-TEM images of SiO_2-TiO_2@propylamine-Ni(II)5

by a lighter color. When the magnification was increased in Fig. 14(b), it can be seen that the SiO_2-TiO_2 as the core is represented by a darker color, propylamine in the outer lighter color, and Ni(II) in the darker layer out of propylamine.

Catalytic Activity Evaluation

According to Fig. 15 and Table 3, it is known that under the same condition, the most active catalyst was SiO_2-TiO_2@propylamine-Ni(II)5, with the yield percentage of 98.52%. It basically confirms that this catalyst had the most nickel ion attached to its surface as the primary catalyst for the oxidation reaction. As a result, the highest activity was achieved, followed by other catalysts with less attached nickel ions. Due to the absence of nickel ion when SiO_2-TiO_2 was used as the catalyst, a product with a lower yield percentage was generated. The product was still formed despite the lack

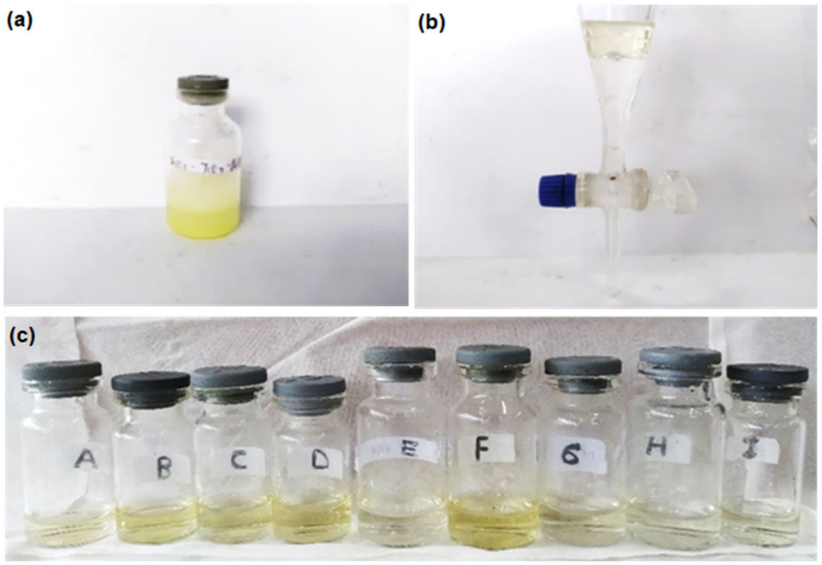

Fig 15. The oxidation reaction of benzyl alcohol to benzaldehyde using SiO_2-TiO_2@propylamine-Ni(II)5, including (a) right after reaction, (b) after catalyst separation, and (c) the products obtained from (A) TiO_2, (B) SiO_2-TiO_2@propylamine, (C) SiO_2-Ni(II), (D) TiO_2-Ni(II), (E) SiO_2-TiO_2@propylamine-Ni(II)3, (F) SiO_2-TiO_2@propylamine-Ni(II)5, (G) SiO_2-TiO_2@propylamine-Ni(II)7, (H) SiO_2-TiO_2@propylamine-Ni(II)10, and (I) SiO_2-TiO_2

Table 3. Oxidation of benzyl alcohol to benzaldehyde

Catalyst	Conversion (%)	Yield (%)	Selectivity (%)
SiO_2	0	0	0
TiO_2	23.44	22.64	96.59
SiO_2-TiO_2@propylamine	33.46	33.46	100
SiO_2-Ni(II)	68.97	67.53	97.91
TiO_2-Ni(II)	58.73	53.52	91.13
Without catalyst	0	0	0
SiO_2-TiO_2	55.45	52.56	94.79
SiO_2-TiO_2@propylamine-Ni(II)3	87.40	87.40	100
SiO_2-TiO_2@propylamine-Ni(II)5	98.62	98.52	99.90
SiO_2-TiO_2@propylamine-Ni(II)7	87.40	87.40	100
SiO_2-TiO_2@propylamine-Ni(II)10	78.91	77.38	98.06

of nickel ion. This is rooted in the fact that in the presence of visible and UV light, TiO_2 was able to carry out the oxidation reaction by breaking H_2O_2 into OH radicals [39]. The OH radicals would help convert benzyl alcohol to benzaldehyde. This phenomenon was also detected in the result obtained when pure TiO_2 was used as the catalyst. The product was still formed caused by the catalytic process that kept occurring due to the photocatalytic activity of TiO_2 itself. Conversely, there was no product observed when pure SiO_2 was used since this material has no catalytic activity [40].

When the functionalized SiO_2-TiO_2 was used as the catalyst, the yield whittled down. As the presence of propylamine from APTES partially covered the SiO_2-TiO_2 surface, causing the interaction between the catalyst and H_2O_2 to be limited. Furthermore, even though the percentage yield of SiO_2-Ni(II) and TiO_2-Ni(II) catalysts is not relatively high, these materials could still convert benzyl alcohol to benzaldehyde. The oxidation reaction was noticed to occur here due to the role of nickel ion as the main metal catalyst.

According to the results, it is known that SiO_2-Ni(II)

outperformed TiO_2-Ni(II) in terms of yield. Due to the large surface area of silica, nickel ion on the surface was more dispersed and avoided agglomeration, which resulted in higher activity than in titania. Contrary to the previous research revealing that titania interacts well with metal catalysts, in this research, titania was observed to have low activity due to its tendency to agglomerate and lower surface area than silica. Meanwhile, when the reaction was conducted without the use of a catalyst, no product was obtained due to the absence of a catalytic process. Table 4 shows some previous studies related to the oxidation reaction of benzyl alcohol to benzaldehyde. Compared to other catalysts that had been evaluated for the same reaction, SiO_2-TiO_2@propylamine-Ni(II) produced considerably better performance, shown by its conversion, yield, and selectivity percentages.

This study tried to propose a mechanism for the oxidation reaction of benzyl alcohol to benzaldehyde using the synthesized catalyst as adapted from Javidfar et al. [2]. The role of Ni(II) in facilitating the oxidation reaction can be observed in Fig. 16, as it utilized its empty orbitals to bind both H_2O_2 as the oxidizing agent and benzyl alcohol as the main reactant. Initially, hydrogen peroxide attached to the empty orbitals of Ni(II), followed by the binding of benzyl alcohol. In succession, a water molecule was formed for one hydroxyl

Table 4. The performance of other catalysts in benzyl alcohol to benzaldehyde oxidation reaction

Catalyst	Yield (%)	References
Ni/Fe_3O_4	99	[7]
$Ni(OH)_2$-modified CdS-MoS_2	94.2	[9]
$[Ni(L)_2(H_2O)_2]$	45.2	[41]
TiO_2/Ti_3C_2	97	[42]
Mesoporous g-C_3N_4	97	[3]
$La(OH)_3/Fe_3O_4$@chitosan	100	[2]
TiO_2 nanorods	58.1	[43]
Ru/g-C_3N_4	72	[5]
SiO_2-TiO_2@propylamine-Ni(II)	98.52	This study

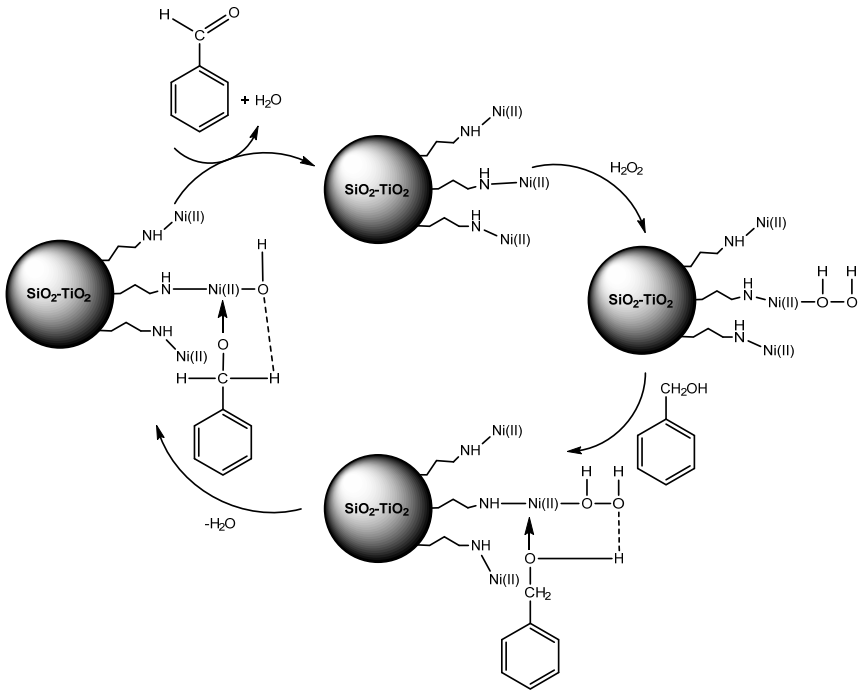

Fig 16. The proposed mechanism of benzyl alcohol to benzaldehyde oxidation reaction using the synthesized catalyst

species from H_2O_2, accepting one hydrogen atom from benzyl alcohol. The remaining hydrogen atom from benzyl alcohol was then bonded with another hydroxyl group from H_2O_2, resulting in the production of water molecules and benzaldehyde as the final products. Throughout this series of oxidation reactions, Ni(II) ultimately returned to its original state, like the one when the reaction had not occurred yet. This route can also be adapted to explain why pure TiO_2 was able to accommodate the oxidation reaction. It is because TiO_2 can produce OH radicals as oxidizing agents due to its photoconductivity [44].

■ CONCLUSION

In this study, we successfully synthesized a new heterogeneous catalyst, namely SiO_2-TiO_2@propylamine-Ni(II). The results of all characterizations synergically report the success of the synthesis. This material was used as the catalyst for benzyl alcohol oxidation reaction as one of the important organic reactions in a wide range of applications. The catalyst has been proven to have excellent performance in oxidation reactions by the presence of H_2O_2 as the oxidizing agent in a sonicated system. Every component in the synthesized catalyst played a significant role in enhancing the catalyst activity. The catalyst was also easy to separate from the product after the reaction was complete. This research results in the development of a potentially new heterogeneous catalyst for organic reactions.

■ ACKNOWLEDGMENTS

The authors would like to acknowledge the Ministry of Research, Technology, and Higher Education Indonesia for funding this research under contract number 089/E5/PG.02.00/PT/2022; 1998/UN1/DITLIT/Dit-Lit/PT.01.03/2022. With respect, we also would like to thank the institution for providing Dewi Agustiningsih the *Pendidikan Magister Menuju Doktor untuk Sarjana Unggul* (PMDSU) scholarship.

■ REFERENCES

[1] Kunene, A., Leteba, G., and van Steen, E., 2022, Liquid phase oxidation of benzyl alcohol over Pt and Pt–Ni alloy supported on TiO_2: Using O_2 or H_2O_2 as oxidant?, *Catal. Lett.*, 152 (6), 1760–1768.

[2] Javidfar, F., Fadaeian, M., and Ghomi, J.S., 2021, $La(OH)_3$ nanoparticles immobilized on Fe_3O_4@ chitosan composites as novel magnetic nanocatalysts for sonochemical oxidation of benzyl alcohol to benzaldehyde, *RSC Adv.*, 11 (57), 35988–35993.

[3] Ramesh, A., Da, C.T., Manigandan, R., Bhargav, P.B., and Nguyen-Le, M.T., 2022, Selectivity oxidation of benzyl alcohol using mesoporous g-C_3N_4 catalysts prepared by hard template method, *Colloid Interface Sci. Commun.*, 48, 100608.

[4] Vásquez-Céspedes, S., Betori, R.C., Cismesia, M.A., Kirsch, J.K., and Yang, Q., 2021, Heterogeneous catalysis for cross-coupling reactions: An underutilized powerful and sustainable tool in the fine chemical industry?, *Org. Process Res. Dev.*, 25 (4), 740–753.

[5] Lima, M.J., Tavares, P.B., Silva, A.M.T., Silva, C.G., and Faria, J.L., 2017, Selective photocatalytic oxidation of benzyl alcohol to benzaldehyde by using metal-loaded g-C_3N_4 photocatalysts, *Catal. Today*, 287, 70–77.

[6] Wu, P., Cao, Y., Zhao, L., Wang, Y., He, Z., Xing, W., Bai, P., Mintova, S., and Yan, Z., 2019, Formation of PdO on Au–Pd bimetallic catalysts and the effect on benzyl alcohol oxidation, *J. Catal.*, 375, 32–43.

[7] Wang, Y., Hu, D., Guo, R., Deng, H., Amer, M., Zhao, Z., Xu, H., and Yan, K., 2022, Facile synthesis of Ni/Fe_3O_4 derived from layered double hydroxides with high performance in the selective hydrogenation of benzaldehyde and furfural, *Mol. Catal.*, 528, 112505.

[8] Hu, X., Zhang, M., Ren, A., Huang, Y., Yan, X., Feng, R., and Zhao, G., 2022, Mesoporous nickel-cobalt oxide for efficient liquid-phase benzyl alcohol oxidation by air, *Catal. Today*, 405-406, 75–81.

[9] Cui, C., Zhao, X., Su, X., Gao, W., Zhan, J., Zhang, X., Li, G., Zhang, X. L., Sang, Y., and Liu, H., 2021, Selective oxidation of benzyl alcohol using a $Ni(OH)_2$-modified CdS-MoS_2 composite photocatalyst under ambient conditions, *J. Environ.*

Chem. Eng., 9 (6), 106416.

[10] Ali, M.E., Rahman, M.M., Sarkar, S.M., and Abd Hamid, S.B., 2014, Heterogeneous metal catalysts for oxidation reactions, *J. Nanomater.*, 2014, 192038.

[11] Bagheri, S., Muhd Julkapli, N., and Bee Abd Hamid, S., 2014, Titanium dioxide as a catalyst support in heterogeneous catalysis, *Sci. World J.*, 2014, 727496.

[12] Deshmukh, P., Bhatt, J., Peshwe, D., and Pathak, S., 2012, Determination of silica activity index and XRD, SEM and EDS studies of amorphous SiO_2 extracted from rice husk ash, *Trans. Indian Inst. Met.*, 65 (1), 63–70.

[13] Setyawan, N., Hoerudin, H., and Yuliani, S., 2021, Synthesis of silica from rice husk by sol-gel method, *IOP Conf. Ser.: Earth Environ. Sci.*, 733, 012149.

[14] Muthukrishnan, S., Gupta, S., and Kua, H.W., 2019, Application of rice husk biochar and thermally treated low silica rice husk ash to improve physical properties of cement mortar, *Theor. Appl. Fract. Mech.*, 104, 102376.

[15] Ozturk, M., Karaaslan, M., Akgol, O., and Sevim, U.K., 2020, Mechanical and electromagnetic performance of cement based composites containing different replacement levels of ground granulated blast furnace slag, fly ash, silica fume and rice husk ash, *Cem. Concr. Res.*, 136, 106177.

[16] Santhosh, K.G., Subhani, S.M., and Bahurudeen, A., 2022, Recycling of palm oil fuel ash and rice husk ash in the cleaner production of concrete, *J. Cleaner Prod.*, 354, 131736.

[17] Avudaiappan, S., Prakatanoju, S., Amran, M., Aepuru, R., Saavedra Flores, E.I., Das, R., Gupta, R., Fediuk, R., and Vatin, N., 2021, Experimental investigation and image processing to predict the properties of concrete with the addition of nano silica and rice husk ash, *Crystals*, 11 (10), 1230.

[18] Qureshi, L.A., Ali, B., and Ali, A., 2020, Combined effects of supplementary cementitious materials (silica fume, GGBS, fly ash and rice husk ash) and steel fiber on the hardened properties of recycled aggregate concrete, *Constr. Build. Mater.*, 263, 120636.

[19] Saloni, S., Parveen, P., and Pham, T.M., 2020, Enhanced properties of high-silica rice husk ash-based geopolymer paste by incorporating basalt fibers, *Constr. Build. Mater.*, 245, 118422.

[20] Hossain, S.S., Roy, P.K., and Bae, C.J., 2021, Utilization of waste rice husk ash for sustainable geopolymer: A review, *Constr. Build. Mater.*, 310, 125218.

[21] Liang, G., Zhu, H., Li, H., Liu, T., and Guo, H., 2021, Comparative study on the effects of rice husk ash and silica fume on the freezing resistance of metakaolin-based geopolymer, *Constr. Build. Mater.*, 293, 123486.

[22] Nana, A., Epey, N., Rodrique, K.C., Deutou, J.G.N., Djobo, J.N.Y., Tomé, S., Alomayri, T.S., Ngouné, J., Kamseu, E., and Leonelli, C., 2021, Mechanical strength and microstructure of metakaolin/volcanic ash-based geopolymer composites reinforced with reactive silica from rice husk ash (RHA), *Materialia*, 16, 101083.

[23] Handayani, L., Aprilia, S., Abdullah, A., Rahmawati, C., Aulia, T.B., Ludvig, P., and Ahmad, J., 2022, Sodium silicate from rice husk ash and their effects as geopolymer cement, *Polymers*, 14 (14), 2920.

[24] Steven, S., Restiawaty, E., Pasymi, P., and Bindar, Y., 2021, An appropriate acid leaching sequence in rice husk ash extraction to enhance the produced green silica quality for sustainable industrial silica gel purpose, *J. Taiwan Inst. Chem. Eng.*, 122, 51–57.

[25] Nayak, P.P., and Datta, A.K., 2021, Synthesis of SiO_2-nanoparticles from rice husk ash and its comparison with commercial amorphous silica through material characterization, *Silicon*, 13 (4), 1209–1214.

[26] Zainal, N.S., Mohamad, Z., Mustapa, M.S., Badarulzaman, N.A., and Zulkifli, A.Z., 2019, The ability of crystalline and amorphous silica from rice husk ash to perform quality hardness for ceramic water filtration membrane, *Int. J. Integr. Eng.*, 11 (5), 229–235.

[27] Fatimah, I., Said, A., and Hasanah, U.A., 2015, Preparation of TiO_2-SiO_2 using rice husk ash as silica source and the kinetics study as photocatalyst in methyl violet decolorization, *Bull. Chem. React. Eng. Catal.*, 10 (1), 43–49.

[28] Prabha, S., Durgalakshmi, D., Rajendran, S., and Lichtfouse, E., 2021, Plant-derived silica nanoparticles and composites for biosensors, bioimaging, drug delivery and supercapacitors: A review, *Environ. Chem. Lett.*, 19 (2), 1667–1691.

[29] Jamwal, B., Kaur, M., Sharma, H., Khajuria, C., Paul, S., and Clark, J.H., 2019, Diamines as interparticle linkers for silica-titania supported PdCu bimetallic nanoparticles in Chan-Lam and Suzuki cross-coupling reactions, *New J. Chem.*, 43 (12), 4919–4928.

[30] Mardjan, M.I.D., Hariadi, M.F., Putri, I.M., Musyarrofah, N.A., Salimah, M., Priatmoko, P., Purwono, B., and Commeiras, L., 2022, Ultrasonic-assisted-synthesis of isoindolin-1-one derivatives, *RSC Adv.*, 12 (29), 19016–19021.

[31] Bai, Y., Li, Z., Cheng, B., Zhang, M., and Su, K., 2017, Higher UV-shielding ability and lower photocatalytic activity of TiO_2@SiO_2/APTES and its excellent performance in enhancing the photostability of poly(*p*-phenylene sulfide), *RSC Adv.*, 7 (35), 21758–21767.

[32] Harraz, F.A., 2008, Polyethylene glycol-assisted hydrothermal growth of magnetite nanowires: Synthesis and magnetic properties, *Phys. E*, 40 (10), 3131–3136.

[33] Kumar, P., Khanduri, H., Pathak, S., Singh, A., Singh, A., Basheed, G.A., and Pant, R.P., 2020, Temperature selectivity for single phase hydrothermal synthesis of PEG-400 coated magnetite nanoparticles, *Dalton Trans.*, 49 (25), 8672–8683.

[34] Netzahual-Lopantzi, Á., Sánchez-Ramírez, J.F., Jiménez-Pérez, J.L., Cornejo-Monroy, D., López-Gamboa, G., and Correa-Pacheco, Z.N., 2019, Study of the thermal diffusivity of nanofluids containing SiO_2 decorated with Au nanoparticles by thermal lens spectroscopy, *Appl. Phys. A*, 125 (9), 588.

[35] Eslami, S., Farhangdoost, B., Shahverdi, H., and Mohammadi, M., 2021, Surface grafting of silica nanoparticles using 3-aminopropyl (triethoxysilane) to improve the CO_2 absorption and enhance the gas consumption during the CO_2 hydrate formation, *Greenhouse Gases: Sci. Technol.*, 11 (5), 939–953.

[36] Roe, S.P., Hill, J.O., and Magee, R.J., 1991, An infrared and electronic spectroscopic study of a series of nickel(II) amine complexes, *Monatsh. Chem.*, 122 (6), 467–478.

[37] Ning, X., Lu, Y., Fu, H., Wan, H., Xu, Z., and Zheng, S., 2017, Template-mediated Ni(II) dispersion in mesoporous SiO_2 for preparation of highly dispersed Ni catalysts: Influence of template type, *ACS Appl. Mater. Interfaces*, 9 (22), 19335–19344.

[38] Tian, Y., Jiao, W., Liu, P., Song, S., Lu, Z., Hirata, A., and Chen, M., 2019, Fast coalescence of metallic glass nanoparticles, *Nat. Commun.*, 10 (1), 5249.

[39] Haghighi, M., and Gooneh-Farahani, S., 2020, Insights to the oxidative desulfurization process of fossil fuels over organic and inorganic heterogeneous catalysts: Advantages and issues, *Environ. Sci. Pollut. Res.*, 27 (32), 39923–39945.

[40] Babyszko, A., Wanag, A., Sadłowski, M., Kusiak-Nejman, E., and Morawski, A.W., 2022, Synthesis and characterization of SiO_2/TiO_2 as photocatalyst on methylene blue degradation, *Catalysts*, 12 (11), 1372.

[41] Wang, L.H., Kong, F.Y., and Tai, X.S., 2022, Synthesis, structural characterization of a new Ni(II) complex and its catalytic activity for oxidation of benzyl alcohol, *Bull. Chem. React. Eng. Catal.*, 17 (2), 375–382.

[42] Bao, X., Li, H., Wang, Z., Tong, F., Liu, M., Zheng, Z., Wang, P., Cheng, H., Liu, Y., Dai, Y., Fan, Y., Li, Z., and Huang, B., 2021, TiO_2/Ti_3C_2 as an efficient photocatalyst for selective oxidation of benzyl alcohol to benzaldehyde, *Appl. Catal., B*, 286, 119885.

[43] Qayyum, A., Giannakoudakis, D.A., LaGrow, A.P., Bondarchuk, O., Łomot, D., and Colmenares, J.C., 2022, High-frequency sonication for the synthesis of nanocluster-decorated titania nanorods: Making a better photocatalyst for the selective oxidation of monoaromatic alcohol, *Catal. Commun.*, 163, 106406.

[44] Hikmah, N., Agustiningsih, D., Nuryono, N., and Kunarti, E.S., 2022, Preparation of iron-doped SiO_2/TiO_2 using silica from sugarcane bagasse ash for visible light degradation of Congo Red, *Indones, J. Chem.*, 22 (2), 402–412.